Extracellular voltage threshold settings can be tuned for optimal encoding of movement and stimulus parameters

Extracellular voltage threshold settings can be tuned for optimal encoding of movement and stimulus parameters

Emily R Oby[1,2], Sagi Perel[1,3], Patrick T Sadtler[1,2], Douglas A Ruff[1,4], Jessica L Mischel[1,2], David F Montez[1,4], Marlene R Cohen[1,4], Aaron P Batista[1,2,5] and Steven M Chase[1,3,5]

[1] Center for the Neural Basis of Cognition, University of Pittsburgh and Carnegie Mellon University, Pittsburgh, PA 15213, USA
[2] Department of Bioengineering, University of Pittsburgh, Pittsburgh, PA 15261, USA
[3] Department of Biomedical Engineering, Carnegie Mellon University, Pittsburgh, PA 15213, USA
[4] Department of Neuroscience, University of Pittsburgh, Pittsburgh, PA 15260, USA

E-mail: schase@cmu.edu

CrossMark

Abstract

Objective. A traditional goal of neural recording with extracellular electrodes is to isolate action potential waveforms of an individual neuron. Recently, in brain–computer interfaces (BCIs), it has been recognized that threshold crossing events of the voltage waveform also convey rich information. To date, the threshold for detecting threshold crossings has been selected to preserve single-neuron isolation. However, the optimal threshold for single-neuron identification is not necessarily the optimal threshold for information extraction. Here we introduce a procedure to determine the best threshold for extracting information from extracellular recordings. We apply this procedure in two distinct contexts: the encoding of kinematic parameters from neural activity in primary motor cortex (M1), and visual stimulus parameters from neural activity in primary visual cortex (V1). *Approach.* We record extracellularly from multi-electrode arrays implanted in M1 or V1 in monkeys. Then, we systematically sweep the voltage detection threshold and quantify the information conveyed by the corresponding threshold crossings. *Main Results.* The optimal threshold depends on the desired information. In M1, velocity is optimally encoded at higher thresholds than speed; in both cases the optimal thresholds are lower than are typically used in BCI applications. In V1, information about the orientation of a visual stimulus is optimally encoded at higher thresholds than is visual contrast. A conceptual model explains these results as a consequence of cortical topography. *Significance.* How neural signals are processed impacts the information that can be extracted from them. Both the type and quality of information contained in threshold crossings depend on the threshold setting. There is more information available in these signals than is typically extracted. Adjusting the detection threshold to the parameter of interest in a BCI context should improve our ability to decode motor intent, and thus enhance BCI control. Further, by sweeping the detection threshold, one can gain insights into the topographic organization of the nearby neural tissue.

Keywords: primate, brain–computer interface, multielectrode, neural prosthetics, motor cortex

(Some figures may appear in colour only in the online journal)

---

[5] Denotes equal contribution.

Introduction

Brain–computer interfaces (BCIs) extract information about motor intentions from recordings of neural signals to control an external device, with the goal of assisting patients with paralysis or other sensory–motor deficits. The recorded signals have taken the form of EEG, MEG, and intracortical signals (Schwartz *et al* 2006). A promising class of BCIs extracts information directly from action potentials, or 'spikes', identified from the voltage traces recorded from chronically implanted extracellular electrodes. To identify these spikes, the voltage trace is typically band-pass filtered, thresholded to identify transients in the voltage signal, and then sorted based on the shape of the transient waveform into clusters corresponding to individual neurons. This final pre-processing step, 'spike sorting', has received considerable attention because it is time consuming, prone to inaccuracies, and difficult to perform in clinical settings (Lewicki 1998, Rey *et al* 2015). Fortunately, it appears that accurate spike sorting may not be necessary for good BCI performance (Ventura 2008, Fraser *et al* 2009, Chestek *et al* 2011, Malik *et al* 2014). Rather, a threshold can be set, and all voltage transients that exceed that threshold (that is, 'threshold crossings') can be counted, regardless of the waveform shape. Evidence is accumulating that there is information in such non-spike signals recorded from microelectrodes. In one example, Stark and Abeles (2007) used a multiunit activity signal, processed by computing the root mean square of the voltage signal in the 300–6000 Hz frequency band, to predict reach direction and grasp with better accuracy than either spike activity or local field potentials. With this knowledge, some researchers have investigated the possibility of moving away from using sorted units as inputs to BCI decoders and instead using threshold crossings (Fraser *et al* 2009). Many studies agree that BCI performance is substantially degraded when the non-spike parts of the signal are discarded (Kloosterman *et al* 2014, Todorova *et al* 2014, Deng *et al* 2015), raising the intriguing possibility that the threshold could be adjusted to maximize BCI performance.

Here we assess how the voltage detection threshold setting ('threshold') affects the encoding of movement parameters in primary motor cortex (M1). We then assess the generality of this approach by using it to examine the information present in recordings from primary visual cortex (V1). To interpret our observations, we reason that the choice of threshold impacts the effective sampling radius of the electrode. For example, choosing a more permissive threshold presumably enlarges the effective sampling radius of the electrode and, thus increases the number of neurons contributing to the threshold crossing signal (Martinez *et al* 2009, Pedreira *et al* 2012). At high detection thresholds, threshold crossings comprise the spikes from individual neurons close to the electrode. At low detection thresholds, threshold crossings comprise multi-unit activity from smaller neurons or neurons farther from the electrode. How the detection threshold is chosen impacts the neural contributions to the signal, and potentially, what information is contained in the signal.

Traditionally, thresholds have been chosen to maximize spike-sorting performance. However, the optimal threshold for single-neuron identification is not necessarily the optimal threshold for information extraction. We hypothesized that the optimal threshold would depend on the parameter of interest. We assessed the impact of the detection threshold by systematically sweeping the detection threshold and evaluating the information content of threshold crossings about two different parameters of interest, velocity and speed, recorded from primary motor cortex (M1). We find that the type of information encoded by threshold crossings depends strongly on threshold, and the optimal threshold depends on the parameter of interest. In particular, we find that velocity, a directional parameter, is better represented at higher thresholds, whereas speed, a scalar quantity, is better represented at lower thresholds. Additionally, we show that optimal thresholds are surprisingly low, considerably below the thresholds commonly used in closed-loop BCI studies. This means that the optimal thresholds for extracting information are not typically the best thresholds for isolating single neurons.

We can understand these results in the context of the topographical representation of speed and velocity in M1. The scale of the topographic organization and the homogeneity of a parameter's representation across cortical tissue influence the optimal threshold. This observation could generalize to other areas of cortex, such that knowledge of the topographic representation of different parameters should predict the choice of threshold for maximizing the information available in neural recordings. We tested this hypothesis with recordings from V1, a cortical area with a distinctly different topographical representation of its relevant parameters. By applying our method of sweeping the threshold, we were able to predict the relative optimal thresholds for the parameters orientation and contrast of a visual stimulus. We conclude that the *type* and *quality* of information that can be extracted from extracellular signals depends on the threshold setting; there is more information present in extracellular voltage recordings than is typically extracted.

Methods

All animal procedures complied with the National Institutes of Health Guide for Care and Use of Laboratory Animals, and were approved by the University of Pittsburgh's Animal Care and Use Committee. To assess the generality of our predictions, we analyzed data collected from two different cortical areas in two monkeys each, and in the context of two different behaviors.

M1 task and recordings

Two male monkeys (Macaca mulatta, 11.6 and 7.3 kg) were trained to perform an 8-target center-out reach task (figure 1(a)). The position of an LED marker attached to the fingertip of the reaching hand was tracked at 120 Hz (<1 mm resolution; Phasespace Inc., San Leandro, CA). The position
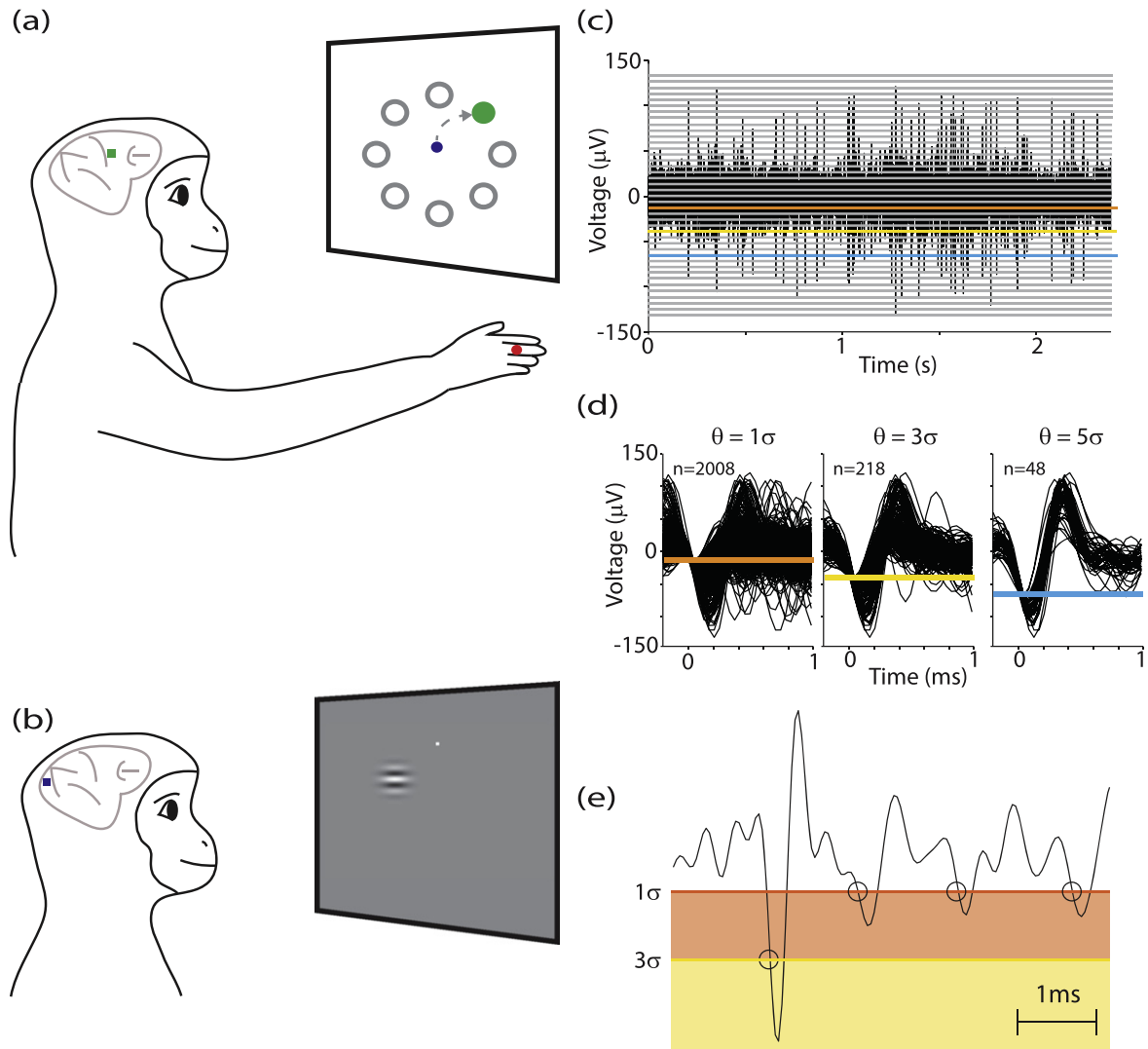
Figure 1. Schematic of tasks and neural recordings. (a) During the M1 recordings, a monkey performed an 8-target center-out reaching task. An LED marker (red) was attached to the monkey's finger tip to track his movements, which were displayed as a cursor on the screen (blue). The monkey made reaches from the center of the screen to one (green) of eight peripheral targets (gray). The array placement in M1 is shown by the green square. (b) During the V1 recordings, a monkey fixated on a central spot (white) while drifting Gabor patches were presented peripherally. The array placement in V1 is shown by the blue square. (c) Voltage trace from M1 during a single reach trial with detection threshold settings from $\theta = 10\sigma$ to -10σ. $\theta = 1\sigma$ (orange) is permissive, capturing low voltage transients. $\theta = 5\sigma$ (light blue) is more restrictive, capturing only high voltage transients which likely correspond to spikes from a single neuron. (d) Waveform snippets for threshold crossings of 1σ, 3σ, and 5σ in C. As the threshold becomes more permissive (1σ, orange) there are more threshold crossings. As the threshold becomes more selective (5σ, light blue) the waveform becomes more consistent. (e) Using the exclusive window categorization method, threshold crossings for the channel are identified when the voltage trace passes into and out of the window defined by a particular threshold without passing into higher-threshold windows. A 1σ window (orange) and a 3σ window (yellow) are shown in this example. If the voltage trace crosses the 1σ threshold but not the 3σ threshold, it is classified as a 1σ crossing. As indicated with the black circles, we can successfully select the larger voltage fluctuations with the exclusive $\theta = 3\sigma$ and we capture the smaller fluctuations with the exclusive $\theta = 1\sigma$.

of the marker was visible to the monkey as a cursor on a frontoparallel screen. The hand was not visible to the monkey, because it moved in the space behind the screen. At the start of each trial, the monkey had to move the cursor to a central target and hold for 200–400 ms. Then, one of eight peripheral targets (arranged at 45° intervals and spaced 9 cm from the center) appeared, and he had ∼800 ms to acquire it with the cursor. After holding the cursor on the peripheral target for 200–500 ms (randomized) he received a liquid reward. A failure at any point caused the trial to terminate without

reward, and there was a 1.5 s timeout before the next trial began.

When the monkey was proficient at the task, we implanted a 96-electrode array (Blackrock Microsystems) in the arm area of M1 (as determined intraoperatively via cortical landmarks) contralateral to the reaching hand (figure 1(a)). As the monkey performed the task we recorded neural data from M1 using a Tucker-Davis Technologies RZ2 system. During each recording session, we streamed the filtered broadband signal (700–3000 Hz band-pass, Kaiser

window) from 4 to 10 different channels directly to disk at a 24 kHz sampling rate. In some cases we streamed an unfiltered broadband signal at a 24 kHz sampling rate and applied a 700–3000 Hz bandpass filter offline. Because of system limitations, we could not record broadband signals from all 96 channels each day. In total, we recorded 20 unique channels over 5 experimental sessions from monkey J (26 months post-implant) and 53 unique channels over 9 experimental sessions from monkey L (2 weeks to 9 months post-implant).

In this data set, we analyzed the representation of two kinematic parameters—velocity and speed—which are known to correlate well with neural firing in M1 (Moran and Schwartz 1999, Churchland and Shenoy 2007, Golub *et al* 2014).

V1 stimuli and recordings

Two different male monkeys (Macaca mulatta, 9.25 and 8.0 kg) were trained to fixate on a central spot while visual stimuli were presented peripherally (figure 1(b)). The animals had been trained to perform an orientation change detection task over the course of several months and were able to stably maintain fixation for 3–5 s. Before electrophysiological recording, the animals were implanted with a custom titanium head post, and a 96-electrode array (Blackrock Microsystems) in V1 (as determined by cortical landmarks, figure 1(b)). Eye position was monitored using an infrared optical recording system (Eyelink, SR Research) sampling at 1 kHz.

To begin each trial, the monkey would acquire fixation on a central spot. After 200–400 ms of stable fixation within a 1 degree window, stimulus presentation began. A total of seven stimuli were flashed for 200 ms each with an interstimulus interval of 100 ms. If the animal maintained fixation for the duration of the stimulus presentations, he was rewarded with a drop of juice. If the animal's eye position left the fixation window during stimulus presentation, the trial was aborted and no reward was given. Stimuli were presented on a mean gray luminance screen (1024 × 768; 27.9 pixels/degree; 120 Hz refresh rate) placed 635 mm in front of the animal. The stimuli were drifting oriented Gabor patches that varied in contrast (contrast values = 0.06, 0.12, 0.25, 0.5, 1) or orientation (orientation values ranged from 0° to 330° in 30° intervals). When orientation was varied, contrast = 1. When contrast was varied, orientation = 90° for monkey B and 180° for monkey G. The receptive fields of the V1 neurons recorded on the array were located approximately 3.5° eccentric from fixation, in the lower right visual field, and they spanned approximately 2° of visual angle. Spatial dimensions of the stimuli were selected to envelop the receptive fields of all V1 neurons recorded by the array. In the initial frame of each stimulus, the grating had odd spatial symmetry. The phase velocity of the stimulus was selected so that upon presentation of the final frame, the stimulus had drifted one complete cycle.

Electrophysiological recordings were performed 2.5 months (monkey B) and 2 weeks (monkey G) post-implant. Data were collected with a Grapevine system (Ripple, Inc.). Broadband signals were recorded on all 96 channels on one day. Each channel was sampled at 30 kHz and raw signals were bandpass filtered (highpass filter: 0.3 Hz; lowpass filter: 7.5 kHz, 3rd order Butterworth) and streamed to disk. The saved signals were subsequently filtered offline in the same way that the M1 signals were, using a Kaiser window with a 700–3000 Hz passband.

In this task, we analyzed the neural representation of the orientation and contrast of the drifting Gabor patch stimulus. Both of these parameters are known to drive neural firing in V1 (Hubel and Wiesel 1959).

Threshold crossings

Our central analysis assesses the information content present in neural recordings at varying voltage thresholds. To do this, we systematically swept the level of the voltage detection threshold to extract threshold crossings (figure 1(c)). At each threshold we evaluated the signal-to-noise ratio (SNR) of the information about movement or stimulus parameters encoded by the corresponding threshold crossings. We defined threshold settings with respect to the standard deviation of the filtered signal (σ), computed as the average standard deviation of the recording over 100–200 trials. We considered threshold settings ranging from 0 (mean) to -10σ for the M1 data and -6σ for the V1 data, at intervals of 0.5σ. These negative threshold settings correspond with the depolarizing phase of the action potential. Results from positive-going thresholds were comparable, and thus we use only the negative thresholds in our analyses. We defined a threshold crossing as the time at which the recorded signal crossed the threshold voltage in a negative-going direction, with 100 μs resolution. For clarity, figures and the following text will refer to the absolute value of the multiplier of the threshold setting (e.g. 3σ).

Quantifying information content with SNR

We use signal-to-noise ratio (SNR) to quantify the information content conveyed by the threshold crossings. Intuitively, SNR can be thought of as the ratio of useful information to irrelevant information. Formally, 'signal' is defined as the variance in the data that is explained by a parameter of interest (e.g. velocity, speed, orientation or contrast), and 'noise' is defined as the residual, unexplained variance after accounting for that parameter. Here, our recorded data, Y_θ, is the number of threshold crossings recorded at a particular threshold θ. We can decompose the variance in our data, Var$[Y_\theta]$, into a component explained by a stimulus X and a component remaining after accounting for X. This decomposition is exact, and is given by the Law of Total Variance:

$$\mathrm{Var}[Y_\theta] = \mathrm{Var}(E[Y_\theta|X]) + E(\mathrm{Var}[Y_\theta|X]), \qquad (1)$$

where $\mathrm{Var}(E[Y_\theta|X])$ is the variance of the expected value of Y_θ conditioned on X, and $E(\mathrm{Var}[Y_\theta|X])$ is the expected value of the variance of Y_θ conditioned on X. The first term quantifies the variation in Y_θ that is explained by X (i.e., the signal variance); the second quantifies the residual variation in Y_θ that remains after accounting for X (i.e., the noise

variance). The SNR is the ratio of these two quantities:

$$\text{SNR}_\theta \equiv \frac{\text{Var}(E[Y_\theta|X])}{E[\text{Var}(Y_\theta|X)]}. \tag{2}$$

For the M1 studies, the parameters of interest are velocity and speed, which both vary in a continuous fashion over the range of natural reaching movements. To compute the SNR in this case, we first fit linear tuning curves by regressing neural activity against kinematics, and then quantified how well these linear fits accounted for the variance of the threshold crossings with the SNR. We considered a separate encoding model for velocity (equation (3)) and speed (equation (4)), and fit an ordinary linear regression at each threshold setting:

$$y_\theta(t) = b_0 + b_x v_x(t) + b_y v_y(t) + \varepsilon_v(t), \tag{3}$$

$$y_\theta(t) = b_0 + b_s s(t) + \varepsilon_s(t), \tag{4}$$

where $y_\theta(t)$ is the number of threshold crossings for a given threshold in a 100 ms bin centered at time t, $v_x(t)$ and $v_y(t)$ are the x- and y-components of the velocity of the cursor averaged over a 100 ms bin, $s(t)$ is the speed of the cursor averaged over a 100 ms bin, and $\varepsilon(t)$ is an error term that captures deviations from the model. These models can be fit at varying temporal offsets between the neural and kinematic data. We used a 100 ms offset (neural activity leading kinematics) because we have found this offset yields the best correlation with behavior for the data sets analyzed here (Perel *et al* 2015). For each encoding model, we used the model estimates to compute the signal variance and the residuals of the regression to compute the noise variance. As an example, for speed the signal variance is the variance of $b_0 + b_s s(t)$ over all recorded speeds, and the noise variance is the variance of $\varepsilon_s(t)$. Graphical depictions of these quantities are provided in figure 2(c).

For the V1 studies, the parameters of interest are orientation and contrast. Each of these varied over discrete levels in our experiments, and firing rates were measured for multiple repetitions of each particular orientation or contrast. In this case $E[Y_\theta|X]$ and $\text{Var}[Y_\theta|X]$ can be measured directly from the data (as depicted in figure 8(a)), without the need for linear regression.

Although SNR is not a common metric in either M1 or V1 studies, it provides a simple, intuitive metric of information content, it is relatively straightforward to compute, and it allows for relatively direct comparisons across brain areas even when the parameters of interest are quite different. A more common metric of goodness of fit in motor neurophysiology is the coefficient of determination (R^2) (e.g., Georgopoulos *et al* 1982), which is a statistical measure of how well a model approximates the data. Qualitatively our M1 results are the same with either measure. However, since neurons in V1 do not respond in a linear fashion to stimuli of different orientations, the R^2 would have been less appropriate for those data. Another possibility would have been to compute the mutual information between threshold crossings and parameters directly. However, comparisons of mutual information across different stimulus sets are difficult to interpret when those sets are not entropy-matched (Chase and

Young 2008, Golub *et al* 2014). For these reasons, we favor the SNR metric for this study. Finally, we note that SNR values less than one are not uncommon in neural responses, especially when analyzed at fine temporal resolution, and low SNR values still signal the presence of meaningful information.

Exclusive windows approach to spike sorting

We reasoned that the small-amplitude fluctuations of the voltage trace might contain information that was distinct from the information contained in the high-amplitude fluctuations. To this end, we performed an 'exclusive window' analysis. In this analysis, a threshold crossing was registered only if it crossed a defined threshold in the negative direction and re-crossed it in the positive direction before crossing another more-negative threshold (figure 1(e)). With this definition, a given excursion of the voltage trace is exclusively categorized as crossing only one threshold. This is in contrast to our basic threshold analysis in which a threshold crossing that crossed a given threshold was counted at all smaller thresholds as well. To differentiate these choices in the text, we refer to exclusive threshold crossings as xTCs. The exclusive windows can act as a crude approach to spike sorting (Todorova *et al* 2014), when large thresholds are selected. Here we examine two exclusive thresholds: a low threshold at 1σ to select the small voltage fluctuations, and a high threshold, which captures the large voltage fluctuations associated with spikes. We considered two possible high thresholds, 3σ or 4.5σ. Using these xTCs, we repeated the SNR analysis as described above.

Results

Our central finding is that in extracellular recordings the detection threshold can be tuned to maximize information about parameters of interest, with different parameters exhibiting different optimal thresholds. Further, the threshold setting that maximizes information is usually not the setting that yields the best spike sorting. We show this in two cortical areas, with two parameters of interest for each area. Our main focus is on primary motor cortex (M1), where we consider the selection of optimal thresholds for the neural encoding of velocity or speed. To examine the generality of this approach, we also apply it to neural recordings from primary visual cortex (V1), where the parameters of interest are orientation and contrast. In both cases, recordings are collected with 96-electrode arrays. Broadband data are saved, and analyses are conducted offline. For each recorded channel, we swept the voltage detection threshold, and measured the number of threshold crossings at each threshold. At each threshold, we quantified the amount of information about the parameter of interest as a SNR.

Information content depends on threshold

Figure 2(a) shows the density of threshold crossings at a low threshold ($\theta = 1\sigma$) and a high threshold ($\theta = 5\sigma$) during reaches to eight different target directions for an example M1
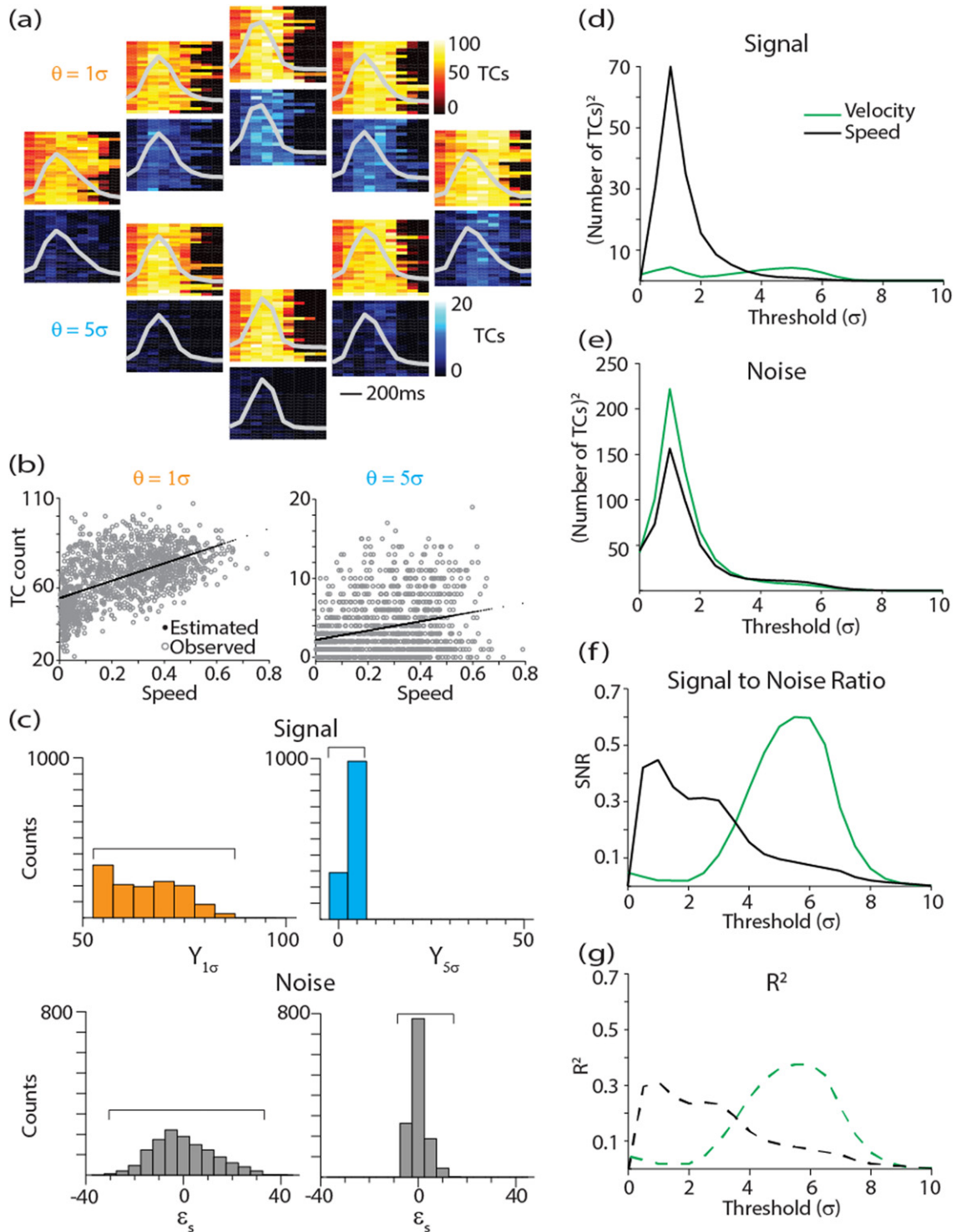
Figure 2. SNR quantifies information content in M1. (a) Single channel example of threshold crossing activity as a function of reach. Each plot shows the number of threshold crossings in 100 ms bins for one of eight reach directions. The color indicates the number of threshold crossings, where the red scale is for $\theta = 1\sigma$ and the blue scale is for $\theta = 5\sigma$. Each row is a trial. The top plots are for a permissive threshold ($\theta = 1\sigma$) and the bottom plots are for a selective threshold ($\theta = 5\sigma$). Average speed profiles for each reach direction are plotted in gray for reference. Note the strong directional tuning for $\theta = 5\sigma$ (with an upwards preferred direction), and the strong speed modulation for $\theta = 1\sigma$. Panels (b)–(f) step through the SNR calculation which we use to quantify this. (b) The observed number of threshold crossings (gray) is plotted against the corresponding reach speed for a permissive (left) and selective (right) threshold. In black, we show the linear regression. (c) We take the variance of Y_θ (as described in equation (4), black in (b)) to be the signal and the variance of the residuals (ε_s as described in equation (4)) to be the noise. The histograms show the distributions of these measurements from which the variance is calculated. The signal (d) and noise (e) arising from these variance calculations vary with threshold. (f) Combining signal and noise, velocity and speed SNRs show an inverted-U shaped relationship with threshold with peaks at different thresholds. (g) A common metric of tuning in M1 is R^2, plotted here for comparison.

channel. It can be seen that different information is manifested in the tuning at different threshold settings. At $\theta = 5\sigma$ (cool color scale), this channel shows velocity tuning, with a preferred direction (PD) up and to the right. At $\theta = 1\sigma$ (warm color scale), this channel modulates similarly for all eight reach directions. The velocity tuning is weak at this threshold, but, instead, the signal reflects speed (gray lines): it is active during the reach regardless of direction. This is an exemplary channel which visually highlights our central finding: by adjusting the threshold setting, we differentially extract information about each parameter (not just different amounts of information about a given parameter) from the neural signal. Separately for each threshold setting, we modeled the relationship between threshold crossings and each kinematic parameter with linear regression. We quantified the information content with the SNR. As an example, figure 2(b) shows the linear regressions for speed at $\theta = 1\sigma$ and $\theta = 5\sigma$. As defined in Methods, the signal is the variance of the estimated threshold crossings and the noise is the variance of the residuals, as shown by the histograms in figure 2(c). We calculated the signal and noise for each threshold setting from 0 to 10σ in 0.5σ increments (figures 2(d) and (e)). Importantly, the SNR depends on the threshold setting (figure 2(f)). Specifically, this channel has more speed information at low thresholds and more velocity information at high thresholds. Perhaps a more familiar metric of goodness of fit in motor neurophysiology is the coefficient of determination (R^2) (e.g., Georgopoulos *et al* 1982). Figure 2(g) plots the dependence of R^2 on threshold. Qualitatively, we see the same dependence of information content on threshold regardless of which measure of goodness of fit we choose. This reassures us that quantification of information with SNR is an appropriate measure for neural recordings from M1, and it has the advantage that it can be applied more broadly to neural recordings from other brain areas.

Figure 3 shows the SNR dependence on threshold for three representative M1 channels. The curves for both speed and velocity show an inverted-U shape with respect to threshold. The lowest SNR values occur at $\theta = 0$, when there are so many threshold crossings that the signal does not provide clear information about the reach kinematics. Similarly, we see low values of SNR at high values of θ, when there are not enough threshold crossings to provide a clear relationship between neural events and the velocity or speed of the reaches. The peak SNR is between these extremes.

From the SNR dependence on threshold we can extract the optimal threshold for velocity and speed information. We computed SNRs for the 73 M1 channels we recorded. We only included a channel in subsequent analyses if it exhibited a statistically significant regression ($\alpha = 0.05$) for at least one threshold setting for at least one of the kinematic parameters. This resulted in 0 discarded channels from monkey J and 6 from monkey L, leaving a total of 20 channels from monkey J and 47 channels from monkey L. The normalized average SNR relationship with threshold for those 67 channels is plotted in figure 4(a). Each channel was normalized to its maximum SNR and then averaged. Normalization emphasizes the relative thresholds at which the peaks occur, regardless of
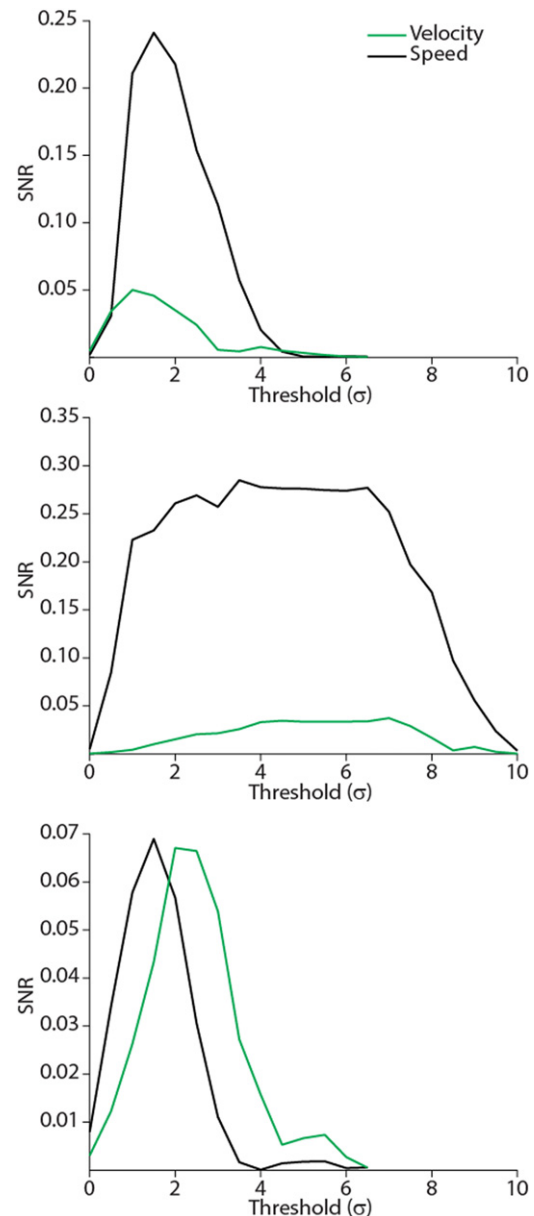

Figure 3. SNR in M1 depends on threshold. SNR dependence on threshold for three representative M1 channels. At each threshold, SNR is computed separately for velocity tuning (green) and for speed tuning (black).

differences in the absolute SNR values across channels. The deviation of the normalized peak from a value of one reflects the variability in the peak threshold across the population. The peak SNR varies for speed and velocity: speed is optimally encoded at a low threshold setting ($\theta = 2\sigma$), while velocity is optimally encoded at higher thresholds ($\theta = 2.5\sigma$). The optimal threshold depends on the information one wishes to extract, and is often lower than the threshold that is typically applied to isolate the activity of a single neuron.

Optimal SNR thresholds are lower than typically used for recording

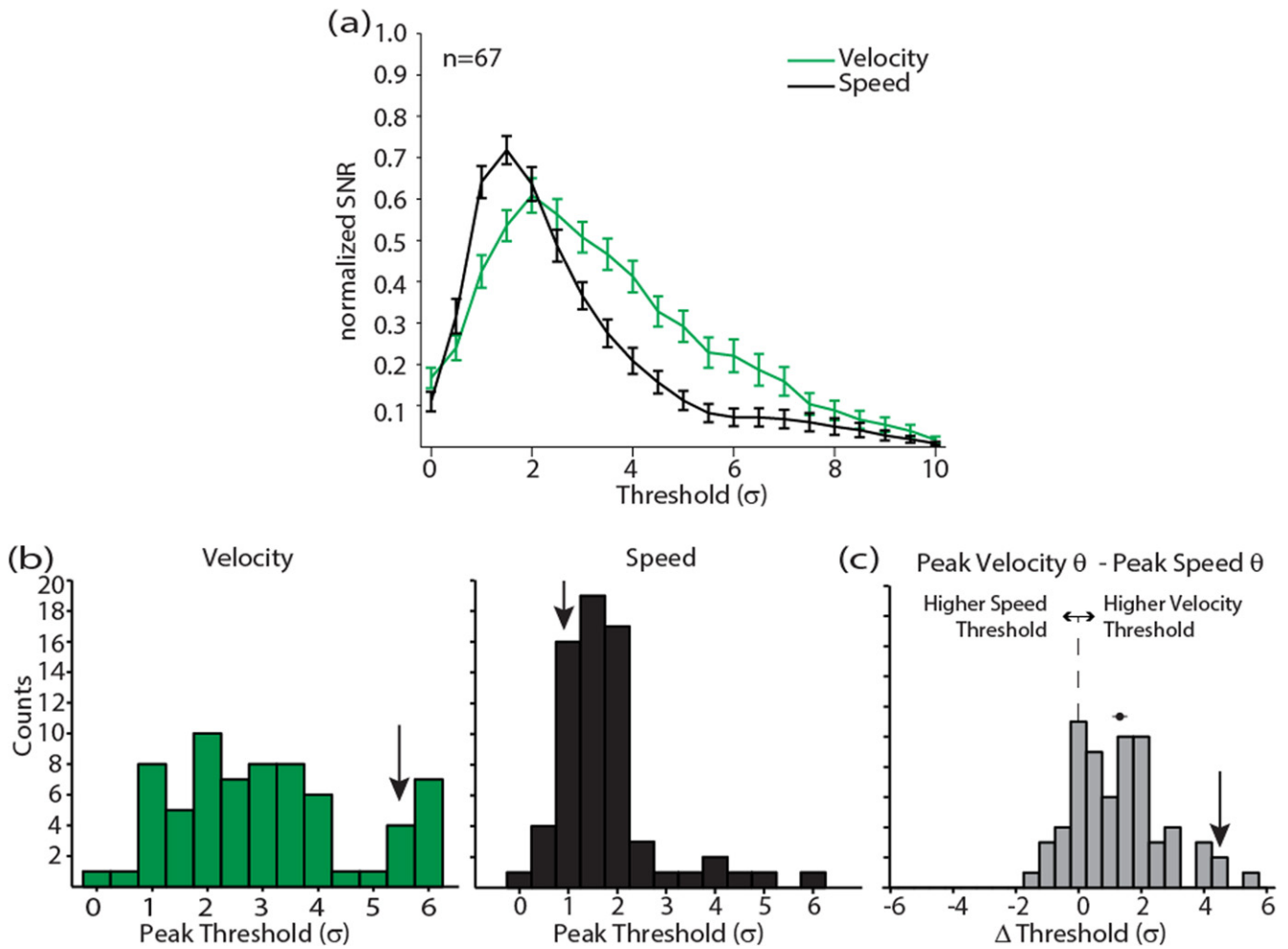In multi-electrode systems where it is possible to adjust the threshold independently for each channel, even more

Figure 4. Optimal thresholds for a given parameter differ across channels. (a) Normalized mean $\pm$ SE of SNR dependence on threshold for all 67 M1 channels with significant tuning. Velocity (green), speed (black). (b) Optimal thresholds for velocity (green) and speed (black). The arrows point to the channel shown in figure 2. (c) The per-channel difference between the optimal thresholds for velocity and speed. The mean $\pm$ SE is indicated by the dot with the line through it above the histogram. The mean is significantly different from zero (*t*-test, $p < 10^{-7}$).

information can be extracted. Figure 4(b) shows histograms for the optimal thresholds for velocity (left) and speed (middle). The distribution of optimal thresholds for speed is narrow with relatively low thresholds. The distribution of optimal thresholds for velocity is broader than is the distribution of optimal thresholds for speed and it includes channels with higher optimal thresholds. The distributions have statistically different means (*t*-test, $p = 10^{-7}$). The mean pairwise difference between the optimal velocity threshold and the optimal speed threshold is $1.28\sigma \pm 0.18\sigma$, and the distribution is shown in the histogram in figure 4(c). The optimal velocity threshold is higher than the optimal speed threshold for 48 of 67 (72%) channels.

Using exclusive thresholds to highlight information content of low amplitude fluctuations

It is conceivable that large-voltage 'spikes' are the sole source of information in an extracellularly recorded signal, and lower thresholds are just capturing these spikes with greater

reliability. Alternatively, the lower amplitude fluctuations which are not readily attributable to the spiking of nearby neurons may contain information that is distinct from that carried by the high-amplitude events. We addressed this through an exclusive threshold analysis. We ask whether single-unit activity and the residual multi-unit hash contribute differently to the speed and velocity encoding models. Figure 5 shows how setting two exclusive thresholds can act as simple spike identifier, using the channel depicted in figure 2 as an example. The black circles identify exclusive threshold crossings (xTCs) for thresholds of 1σ and 3σ. Setting the threshold high has a similar effect as spike sorting, in that it captures single unit activity, whereas the low threshold captures non-single unit activity that might typically be discarded under a sorting paradigm, as evidenced by the waveform snippets shown in figure 5(b). The SNR for the xTCs from this example channel at $\theta = 1\sigma$ shows that there is speed information contained in the non-single unit activity (figure 5(c)). The single unit activity captured by $\theta = 3\sigma$ shows better velocity encoding. This supports the idea that
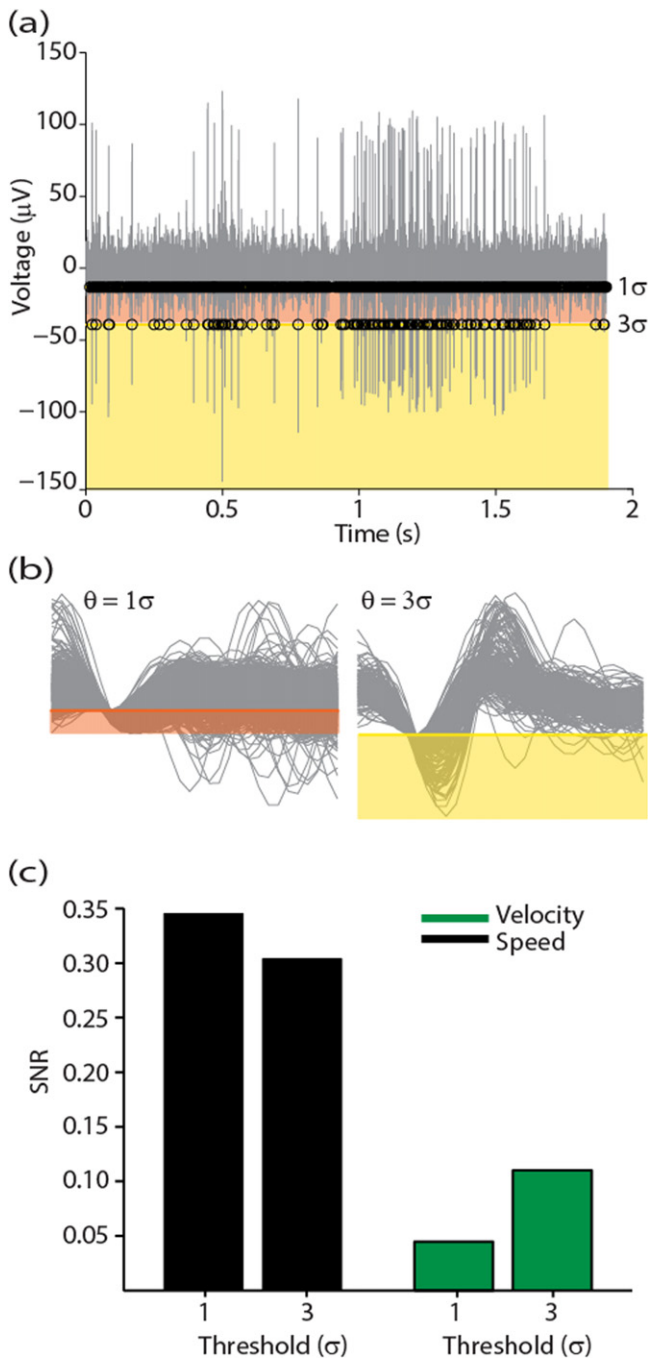
Figure 5. An exclusive window analysis reveals substantial information in small voltage fluctuations. (a) Using the exclusive window categorization method, threshold crossings for the channel depicted in figure 2 are identified when the voltage trace passes into and out of the window defined by a particular threshold without passing into higher-threshold windows. A 1σ window and a 3σ window are shown in this example. If the voltage trace crosses the 1σ threshold but not the 3σ threshold, it is classified as a 1σ crossing. As indicated with the black circles, we can successfully select the larger voltage fluctuations with the exclusive $\theta = 3\sigma$ and we capture the smaller fluctuations with the exclusive $\theta = 1\sigma$. (b) Waveform snippets corresponding to the xTCs for exclusive thresholds $\theta = 1\sigma$ (left) and $\theta = 3\sigma$ (right) for the channel shown in (a). (c) The SNR for velocity and speed at exclusive thresholds $\theta = 1\sigma$ and $\theta = 3\sigma$ for the channel shown in (a). Note that the speed SNR is higher at $\theta = 1$ than $\theta = 3$ even though those waveforms look like noise.

low-voltage events contain information that is distinct from the information present in spiking activity.

The mean exclusive threshold SNR for all channels is shown in figure 6. On average (figure 6(a), left), the non-spike parts of the signal represented by the xTCs at $\theta = 1\sigma$ encode speed better than the xTCs at $\theta = 3\sigma$. Velocity is better encoded at more restrictive (higher) thresholds. To highlight the impact that the choice of threshold has on the information content of the threshold crossings, we repeated the exclusive threshold analysis for M1 at $\theta = 1\sigma$ and $\theta = 4.5\sigma$. Such a high threshold should isolate single units and is thought to obtain better encoding of kinematic information. However, we found that this threshold is quite restrictive and misses some of the available information (figure 6(b)). The exclusive window analysis highlights that there is information contained in the low-amplitude fluctuations of the signal that is often discarded as noise.

Information content in V1

To test the generality of our finding that the optimal threshold depends on the parameter of interest, we examined recordings from primary visual cortex (V1). We selected V1 for comparison in part because its function is markedly different from M1, and also because the topography of V1 is well-established. In V1, nearby neurons are tuned similarly to stimulus orientation, with orientation tuning changing in a systematic way across the cortical surface (Hubel 1982). However, all V1 neurons are tuned similarly to contrast, showing increased firing rates with increasing stimulus contrast (Albrecht and Hamilton 1982). The topographic organization of V1 led us to predict that the optimal threshold for contrast information would be lower than the optimal threshold for orientation information.

We recorded from two monkeys with multi-electrode arrays implanted in V1 while they viewed drifting gratings, and investigated how information about orientation and contrast depended on threshold. The channels were tuned to different orientations, but all channels showed a similar response to contrast, wherein the maximal response was for contrast = 1. Figure 7 plots tuning curves for contrast and orientation at three thresholds for an example channel. Each point in the tuning curve is the number of threshold crossings occurring during a single presentation of a stimulus with a particular orientation or contrast. The mean is plotted to help visualize the tuning.

To test our prediction that orientation and contrast show different optimal thresholds, we calculated the SNR at each threshold to quantify the information content of the threshold crossings. We break down this calculation into its components in figure 8. For orientation, signal is the variance of the mean number of threshold crossings over each orientation (figure 8(a), orange). Noise is the mean of the variance in threshold crossings at each orientation (figure 8(a), black). As shown for this example channel in figure 8(c), orientation and contrast SNR depend on threshold, with both curves showing an inverted-U shape. For this channel, contrast shows a peak
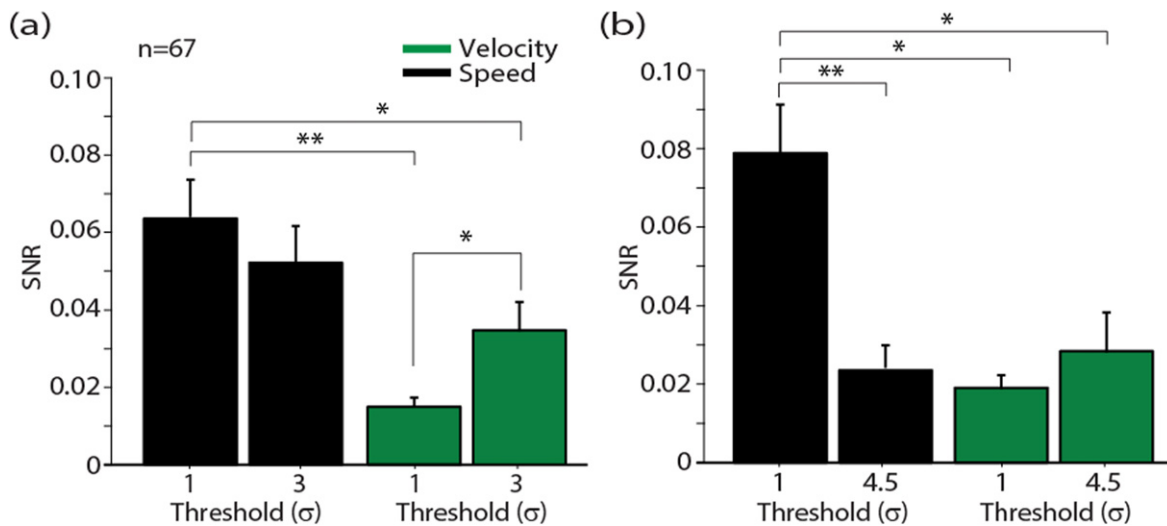
Figure 6. Distinct information is encoded by small and large voltage fluctuations. (a) SNR as a function of exclusive threshold (mean $\pm$ SE). Different information is contained in putative spikes classified with $\theta = 3\sigma$ and in the low voltage fluctuations at $\theta = 1\sigma$. (b) The exclusive window SNR for exclusive windows of $\theta = 1\sigma$ and $\theta = 4.5\sigma$ (a threshold commonly chosen in BCI studies.) It is important to note that because of the exclusive nature of the thresholds, adjusting the high threshold also impacts the xTCs at the low threshold. Thus, the SNR at 1σ changes when the high threshold is different. This is not true for the inclusive thresholds used in the other analyses. (Data are from M1, $n = 67$.) Significant differences are indicated with * for $p < 0.01$ and ** for $p < 10^{-4}$.

SNR at $\theta = 2\sigma$, and orientation shows a peak SNR at $\theta = 2.5\sigma$.

We calculated how SNR depends on threshold for a population of 49 channels (figure 9(a)). Only channels which were well-tuned to orientation (SNR > 0.75) were included in this and subsequent analyses. Every channel that showed a response to the stimulus demonstrated an SNR greater than 0.75 for contrast, and thus we chose the significant channels conservatively, based on orientation tuning. Like the individual channel example, there is an inverted-U shaped curve with the peak occurring between the extremes of too many threshold crossings and too few threshold crossings. The SNR curves for both orientation and contrast depend on threshold similarly, with contrast optimally represented at $\theta = 2\sigma$ and orientation optimally represented at $\theta = 2.5\sigma$ on average for the population.

The optimal threshold histograms for orientation and contrast are plotted in figure 9(b). Both distributions of optimal contrast thresholds and optimal orientation thresholds are narrow with primarily low thresholds. However, the optimal threshold for orientation is higher than the optimal threshold for contrast for 26 of the 49 (53%) channels and the distributions have statistically different means (*t*-test, $p = 0.004$). The mean pairwise difference between the optimal orientation threshold and optimal contrast threshold is $0.35\sigma \pm 0.11\sigma$ (figure 9(c)).

Discussion

We assessed the information content of extracellular recordings from M1 and V1 by systematically sweeping the voltage detection threshold, counting the number of threshold crossing events at that threshold setting, and evaluating how much

information those threshold crossings provided about external parameters of interest. We found that optimal threshold depends on the parameter of interest. Specifically, directional parameters, like velocity and orientation, have higher optimal thresholds than scalar parameters, like speed and contrast. Regardless of the parameter of interest, the optimal thresholds for information were lower than the thresholds typically used in closed-loop BCI studies in which threshold crossings are used in lieu of spike sorting. We can make sense of these observations with a consideration of cortical topography. These results have pragmatic implications for the optimal decoding of neural signals.

Cortical topography can explain optimal thresholds

How a stimulus parameter is represented in an extracellular voltage trace will depend in part on how the topographic scale of tuning to that parameter in the cortex relates to the effective sampling radius of the electrode, as determined by the detection threshold. At high detection thresholds, threshold crossings reflect the tuning of individual neurons. At low detection thresholds, threshold crossings comprise multi-unit activity and tuning likely reflects the homogeneity of the tuning of local neurons. Modeling studies have suggested that single unit activity arises from neurons within 50 μm of an extracellular electrode and multi-unit activity arises within 50–140 μm of the electrode (Martinez *et al* 2009, Pedreira *et al* 2012). Thus, it is reasonable to expect that the topographic scale at which a stimulus parameter is represented impacts threshold crossing tuning, particularly at low thresholds.

Figure 10 schematizes a putative explanation for the effects of threshold selection that we observed. As the detection threshold of an electrode is moved toward 0, its
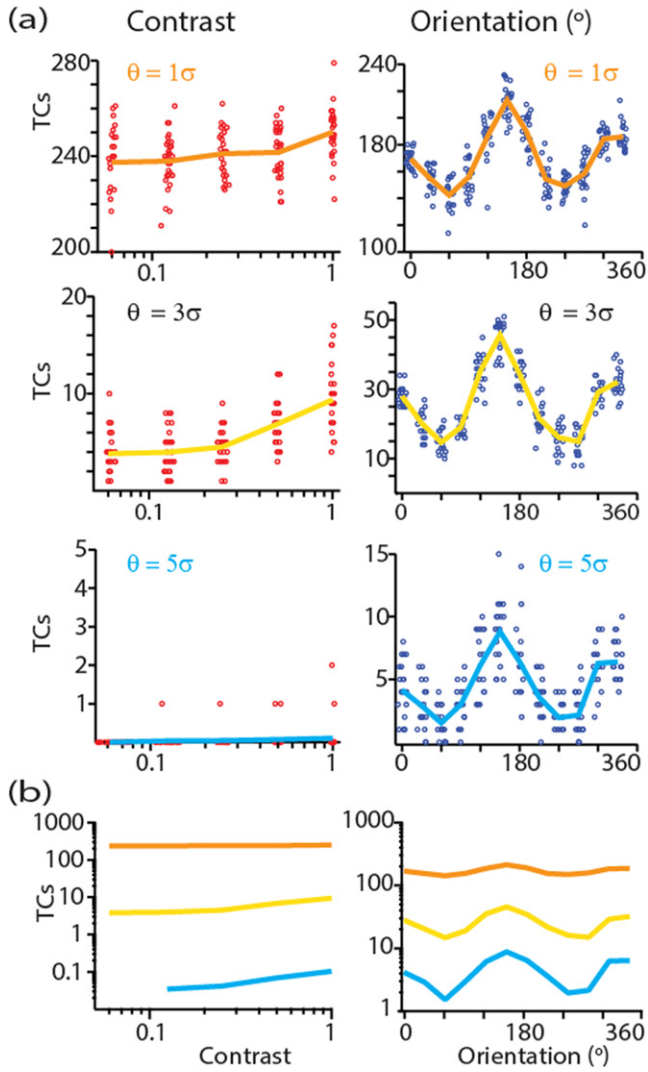
Figure 7. A single V1 channel example of how contrast and orientation tuning change with threshold. (a) Each data point represents the number of threshold crossings from one representative electrode recorded during a single trial. For visualization purposes, the data points are jittered with respect to orientation angle or contrast, respectively. To highlight the tuning, the mean threshold crossings to each orientation are connected and plotted using the color scheme in figure 2 (orange = 1σ, yellow = 3σ, light blue = 5σ). These curves are overlaid on the same plot in (b). Note the log scale on the TC axis.
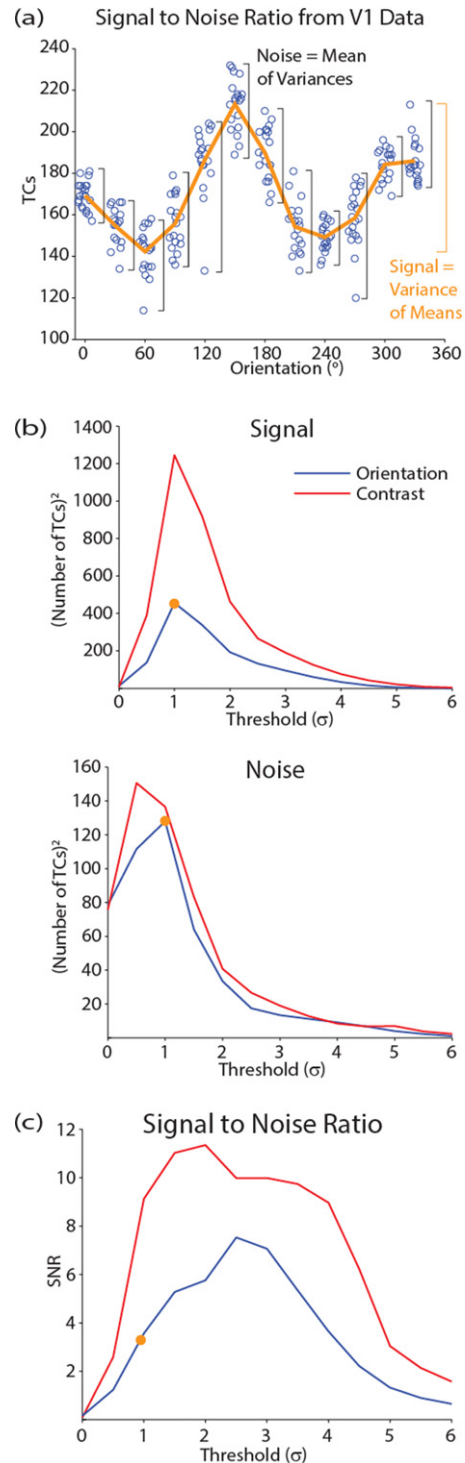

Figure 8. SNR quantifies information content in V1. (a) The total number of threshold crossings is plotted against orientation angle for a single channel at a threshold of $\theta = 1$. (For visualization purposes, the data points are jittered around the true orientation angle.) Signal is defined as the variance of the mean number of threshold crossings across each orientation (orange). Noise is defined as the mean of the variance of the number of threshold crossings across each orientation (black). (b) The calculations are performed at each threshold for orientation (blue) and contrast (red). Signal and noise both vary with threshold setting. The orange dot highlights the values that come from the tuning curve in A. (c) Combining the relationships in B shows that SNR exhibits an inverted-U shaped relationship with threshold.
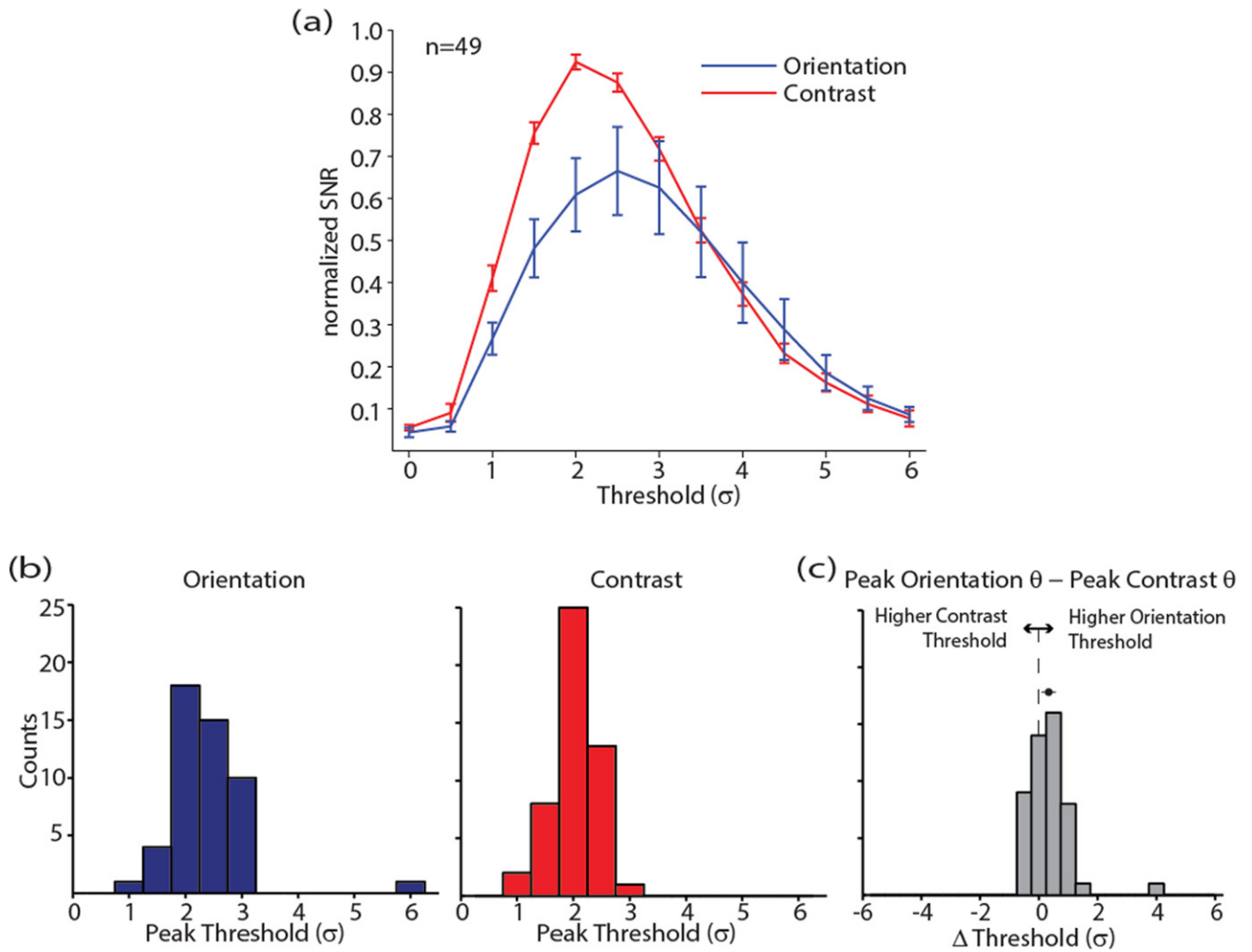
effective sampling radius increases (figure 10(a)). (Note that while the relationship between detection threshold and effective sampling radius is probably not linear, it is likely to be monotonic). As the threshold is lowered, the number of threshold crossings increases, as does the variability in the waveform shapes. A strict threshold, like $\theta = 5\sigma$ (blue), yields waveforms that likely originate from a single neuron. On the other hand, if we relax the threshold to $\theta = 1\sigma$ (orange), the waveforms are almost certainly not from a single unit.

A schematic example of parameters with different topographic scales relative to the 'listening sphere' of an electrode is shown in figure 10(b). Here the black arrows represent a

Figure 9. SNR in V1 depends on threshold. (a) SNR dependence on threshold for orientation (blue) and contrast (red) for all V1 electrodes with significant tuning, $n = 49$ (normalized mean $\pm$ SE). (b) Optimal thresholds for encoding orientation and contrast. (c) The per-channel difference between the optimal thresholds for orientation and contrast. The mean $\pm$ SE is shown above the histogram. The mean is significantly different than 0 (*t*-test, $p = 0.004$), and significance still holds when the outlier at $\Delta\theta = 4\sigma$ is removed ($p = 0.0045$).

directional parameter that has a small tuning scale relative to the listening sphere of the electrode, meaning the correlation in tuning among neurons falls off relatively quickly with distance. The light and dark gray regions represent a parameter that has a large tuning scale relative to the listening sphere of the electrode, meaning the correlation in tuning falls off relatively slowly with distance. The topographic scale of the stimulus parameter impacts the information present in the extracellular recording at different thresholds. At low detection thresholds, threshold crossings comprise multi-unit activity and tuning should better reflect those parameters that are homogeneously encoded among the population of neurons local to the electrode (figure 10(c), gray). In contrast, we expect parameters that are more heterogeneously encoded to be better represented at high detection thresholds, where threshold crossings reflect the tuning of individual neurons (figure 10(c), black). Accordingly, in M1 we observed that velocity has a higher optimal threshold than speed.

The influence of topographic scale on information encoding by threshold crossings

We introduce a conceptual model based on the topographic scale of information encoding to explain our results (figure 10). If we apply that model to V1's pinwheel organization of orientation preference, we should expect a change of $<30°$ for neurons within the putative sampling radius of our electrode at the lowest detection threshold. So, the topographic scale of orientation is on the order of the sampling radius. The topographic scale of contrast is larger than for orientation: nearly all V1 neurons increase their firing with increases in contrast. In accordance with this understanding of V1 topography, we found the optimal orientation threshold to be similar to but slightly larger than the optimal contrast threshold. Additionally, the optimal thresholds in V1 were relatively low, suggesting that including threshold crossings from more neurons provides more information than does a single neuron.
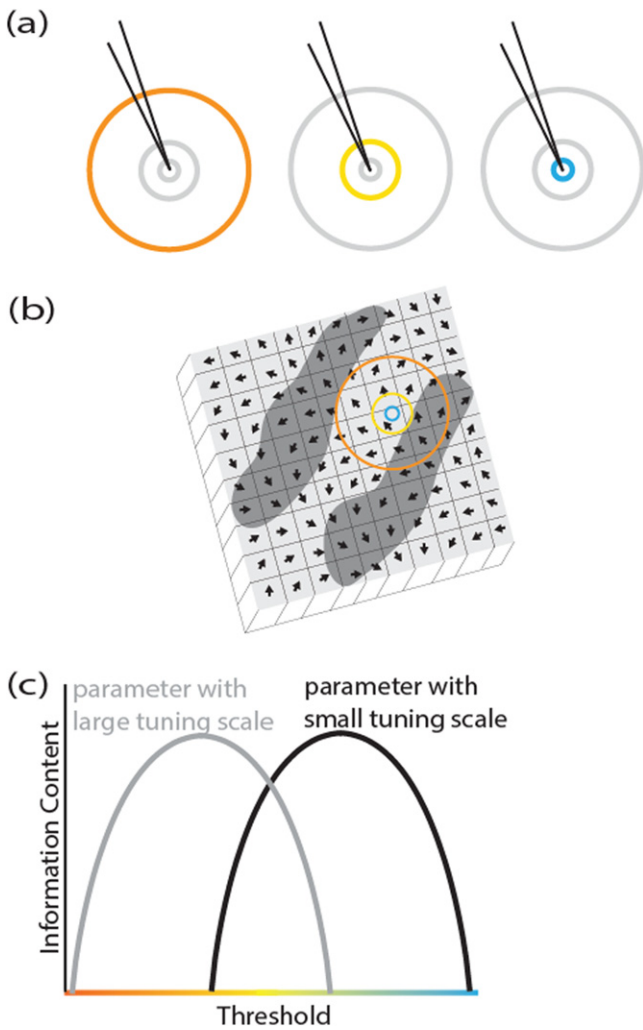
Figure 10. Information content depends on the voltage detection threshold and the topographic scale of the parameter of interest. (a) A change in the detection threshold might change the effective sampling radius of the electrode. As we decrease the detection threshold of an electrode (move from blue to yellow to orange), we increase its effective sampling radius. (b) The relationship between effective sampling radius and the topographic scale of an encoded parameter. The black arrows represent a parameter that is encoded on a small scale. The gray regions represent a parameter that is encoded on a larger scale. The color scheme of the sampling radii is the same as above. (c) The information content of a signal depends on the threshold setting and the local topography such that a parameter encoded on a large scale (gray) has a lower optimal threshold than a parameter encoded on a small scale (black).

The heterogeneity of the local M1 PD map is in stark contrast to the large-scale topography of V1 orientation columns (Schieber and Hibbard 1993). However, in an effort to make sense of the structure of M1, a columnar organization similar to that observed in V1 has been proposed (Amirikian and Georgopoulos 2003). This hypothesized structure of M1 consists of mini-columns of neurons with similar PDs 30 μm in width and repeating every 240 μm (Georgopoulos *et al* 2007). Such structure would lead to a nearly complete set of PDs represented by neurons within the ~200 μm sampling radius of an electrode. This is a far less homogeneous local

structure than that seen in V1. Consistent with this model, at high detection thresholds, velocity is encoded well by threshold crossings. This recapitulates the well-known PD tuning of individual neurons in M1 (Schwartz *et al* 1988). However, within the larger effective sampling radius specified by a low threshold, the diversity of PDs of the contributing neurons weakens the measured velocity tuning. On the other hand, most M1 neurons tune monotonically to speed (Moran and Schwartz 1999). Thus, speed encoding is strongest at low thresholds, since many neurons contribute to the threshold crossings. This can explain our observation of higher optimal thresholds for velocity than for speed.

The information available at low voltage threshold settings is not just a watered-down version of the information available at higher thresholds. Although speed may be thought of as a less specific version of velocity (speed can be derived from velocity, but velocity is not uniquely specified by speed), speed and direction are independent quantities, and when we repeat our analyses using movement direction, we find direction and velocity have similar optimal thresholds (data not shown). Further, contrast cannot be derived from orientation, and we find the best threshold for orientation information is higher than for contrast. The primary characteristic influencing the optimal threshold of a parameter is whether it is represented homogeneously by the cortical population, or heterogeneously. The directional quantities, velocity and orientation, are heterogeneously represented, while the scalar parameters, speed and contrast, are homogenously represented.

Our results imply that even single electrodes might be useful for inferring the topography of tuning properties in brain areas where it is not known. By sweeping the event detection threshold and computing the SNR to various parameters of interest, some notion of the relative homogeneity of tuning to different parameters can be gained. Parameters that drive neurons in a heterogeneous, uncorrelated way over short spatial scales should be best represented at relatively high thresholds. In contrast, parameters whose tuning correlates over larger spatial extents should be better represented at lower thresholds. This knowledge could be critical in designing more effective extracellular recording experiments to reveal the nature of the information present in a given brain area.

Implications for online decoding

In many successful BCIs to date, information is extracted directly from sorted spikes recorded from chronically implanted extracellular electrodes. Although BCIs based on sorted spikes have shown impressive performance both in the lab (Wessberg *et al* 2000, Taylor *et al* 2002, Velliste *et al* 2008, Ethier *et al* 2012, Gilja *et al* 2012, Ifft *et al* 2013) and in controlled clinical trials (Simeral *et al* 2011, Collinger *et al* 2013), spike-sorting is widely acknowledged to be time-consuming, and hard to automate (Lewicki 1998). Because of these challenges, the spike-sorting step, once thought to be critical to BCI performance, may actually inhibit the

translation of BCIs from the lab to the clinic. Here we add to that perspective by showing that better information extraction might be possible if thresholds are tuned for the parameter of interest, rather than set as if for spike sorting. The benefits should be especially salient for electrode channels where no identifiable single neuron is present.

The use of threshold crossings is becoming more prevalent in online decoding studies. This is not surprising given that in offline analyses multiunit activity and threshold crossings have yielded decoding performance and encoding fidelity that is comparable to or better than sorted spikes or local field potentials (Stark and Abeles 2007, Ventura 2008, Chestek *et al* 2011, Kloosterman *et al* 2014, Malik *et al* 2014, Todorova *et al* 2014, Christie *et al* 2015, Perel *et al* 2015). Recently, we and others have begun to recognize the need to investigate threshold setting in a principled way. Christie and colleagues (Christie *et al* 2015) found optimal thresholds for decoding performance to be between 3–4.5 times the rms voltage (V_{rms}). Importantly, they only considered threshold settings from 3–18 $\times$ V_{rms}; they did not consider threshold crossings at lower threshold settings. A separate study by our team included lower voltage fluctuations in their threshold crossings by using an approach similar to the exclusive windows analysis presented here, and found that threshold crossings at $\theta = 3\sigma$ actually improved decoding as compared to only well-sorted spikes (Todorova *et al* 2014). This result corroborates our finding that the low voltage fluctuations are not noise, but rather, they do contain useful information: speed-related information that is distinct from the velocity information present at higher thresholds. For the thresholds and parameters we considered, the optimal thresholds were lower than typically used in online decoding studies (Gilja *et al* 2012, Hochberg *et al* 2012, Sadtler *et al* 2014), suggesting that there is information available in extracellular recordings that is being discarded, and could be useful for improving BCI performance. Ideally, the detection threshold would be customized for each channel. In fact, each channel's signal could be duplicated and thresholded separately for each parameter used in a BCI.

Notably, the thresholds that we found to be optimal are lower than thresholds typically reported in published studies. In M1, particularly for online BCI experiments using threshold crossings, a fixed threshold of $\theta = 4.5\sigma$ is commonly chosen (Gilja *et al* 2012, Hochberg *et al* 2012) presumably because it approximates spike sorting. Some of the best online BCI control has been achieved with this commonly chosen threshold. However, we observed only 14 of 67 (20%) channels that showed optimal velocity thresholds greater than or equal to $\theta = 4.5\sigma$. This was even more apparent for speed, where only three channels had optimal thresholds at the level commonly chosen. Optimal thresholds are likely to depend on many factors, including recording quality and the age of the implant. It stands to reason that even better BCI decoding may be possible if the threshold is chosen with information content in mind.

Conclusions

Historically, neurophysiologists have processed extracellular voltage recordings to extract action potentials from isolated single neurons, essentially ignoring small amplitude voltage fluctuations. This makes sense if the focus is on a careful characterization of the properties of single neurons. However, if the goal is to get as much information as possible from a recorded signal, processing can only reduce available information (Cover and Thomas 1991). Accordingly, we have shown that non-spike parts of the recorded signal, in particular the low voltage fluctuations, include useful information about some parameters, and should not be discarded as noise. Our results suggest that signal preprocessing in neurophysiology experiments deserves careful consideration: one approach does not necessarily fit all applications. For recordings from a given brain area, it would be advantageous to sweep a range of thresholds to find the optimal choice for the desired information and planned experiment. For applications that do not require real-time processing, there is value in streaming the entire raw voltage signal to disk for offline analysis, and then considering the information content at different threshold settings. The practice of adjusting the detection threshold to the parameter of interest may improve our ability to determine how the brain is organized to encode sensory information, and it may improve our ability to accurately decode motor intentions.

Acknowledgements

Conflict of interest

The authors declare no competing financial interests.

References

Albrecht D G and Hamilton D B 1982 Striate cortex of monkey and cat: contrast response function *J. Neurophysiol.* **48** 217–37

Amirikian B and Georgopoulos A P 2003 Modular organization of directionally tuned cells in the motor cortex: is there a short-range order? *Proc. Natl Acad. Sci. USA* **100** 12474–9

Chase S M and Young E 2008 Cues for sound localization are encoded in multiple aspects of spike trains in the inferior colliculus *J. Neurophysiol.* **99** 1672–82

Chestek C A *et al* 2011 Long-term stability of neural prosthetic control signals from silicon cortical arrays in rhesus macaque motor cortex *J. Neural. Eng.* **8** 045005

Christie B P, Tat D M, Irwin Z T, Gilja V, Nuyujukian P, Foster J D, Ryu S I, Shenoy K V, Thompson D E and Chestek C A 2015 Comparison of spike sorting and thresholding of voltage waveforms for intracortical brain–machine interface performance *J. Neural. Eng.* **12** 016009

Churchland M M and Shenoy K V 2007 Temporal complexity and heterogeneity of single-neuron activity in premotor and motor cortex *J. Neurophysiol.* **97** 4235–57

Collinger J L, Wodlinger B, Downey J E, Wang W, Tyler-Kabara E C, Weber D J, McMorland A J, Velliste M, Boninger M L and Schwartz A B 2013 High-performance neuroprosthetic control by an individual with tetraplegia *Lancet* **381** 557–64

Cover T M and Thomas J A 1991 *Elements of Information Theory* (New York: Wiley-Interscience)

Deng X, Liu D F, Kay K, Frank L M and Eden U T 2015 Clusterless decoding of position from multiunit activity using a marked point process filter *Neural Comput.* **27** 1438–60

Ethier C, Oby E R, Baumann M J and Miller L E 2012 Restoration of grasp following paralysis through brain-controlled stimulation of muscles *Nature* **485** 361–5

Fraser G W, Chase S M, Whitford A S and Schwartz A B 2009 Control of a brain–computer interface without spike sorting *J. Neural Eng.* **6** 055004

Georgopoulos A P, Kalaska J F, Caminiti R and Massey J T 1982 On the relations between the direction of two-dimensional arm movements and cell discharge in primate motor cortex *J. Neurosci.* **2** 1527–37

Georgopoulos A P, Merchant H, Naselaris T and Amirikian B 2007 Mapping of the preferred direction in the motor cortex *Proc. Natl Acad. Sci. USA* **104** 11068–72

Gilja V *et al* 2012 A high-performance prosthesis enabled by control algorithm design *Nat. Neurosci.* **15** 1752–7

Golub M D, Yu B M, Schwartz A B and Chase S M 2014 Motor cortical control of movement speed with implications for brain–machine interface control *J. Neurophysiol.* **112** 411–29

Hochberg L R *et al* 2012 Reach and grasp by people with tetraplegia using a neutrally controlled robotic arm *Nature* **485** 372–5

Hubel D H 1982 Exploration of the primary visual cortex, 1955–78 *Nature* **299** 515–24

Hubel D H and Wiesel T N 1959 Receptive fields of single neurons in the cat's striate cortex *J. Physiol.* **148** 574–91

Ifft P J, Shokur S, Lebedev M A and Nicolelis M A 2013 A brain–machine interface enables bimanual arm movements in monkeys *Sci. Transl. Med.* **5** 210ra154

Kloosterman F, Layton S P, Chen Z and Wilson M A 2014 Bayesian decoding using unsorted spikes in the rat hippocampus *J. Neurophysiol.* **111** 217–27

Lewicki M S 1998 A review of methods for spike sorting: the detection and classification of neural action potentials *Network* **9** R53–78

Malik W Q, Donoghue J P and Hochberg L R 2014 Decoding analog multiunit activity in a brain–machine interface for individuals with tetraplegia *Paper presented at the IEEE Engineering in Medicine and Biology Society Conf. (Chicago, IL, 14 August)*

Martinez J, Pedreira C, Ison M J and Quian Quiroga R 2009 Realistic simulation of extracellular recordings *J. Neurosci. Methods* **184** 285–93

Moran D W and Schwartz A B 1999 Motor cortical representation of speed and direction during reaching *J. Neurophysiol.* **82** 2676–92

Pedreira C, Martinez J, Ison M J and Quian Quiroga R 2012 How many neurons can we see with current spike sorting algorithms? *J Neurosci. Methods* **211** 58–65

Perel S, Sadtler P T, Oby E R, Ryu S I, Tyler-Kabara E C, Batista A P and Chase S 2015 Single-unit activity, threshold crossings, and local field potentials in motor cortex differentially encode reach kinematics *J. Neurophysiol.* **114** 1500–12

Rey H G, Pedreira C and Quian Quiroga R 2015 Past, present and future of spike sorting techniques *Brain Res Bull.* **119** 106–17

Sadtler P T, Quick K M, Golub M D, Chase S M, Ryu S I, Tyler-Kabara E C, Yu B M and Batista A P 2014 Neural constraints on learning *Nature* **512** 423–6

Schieber M H and Hibbard L S 1993 How somatotopic is the motor cortex hand area? *Science* **261** 489–92

Schwartz A B, Cui X T, Weber D J and Moran D W 2006 Brain-controlled interfaces: movement restoration with neural prosthetics *Neuron* **52** 205–20

Schwartz A B, Kettner R E and Georgopoulos A P 1988 Primate motor cortex and free arm movements to visual targets in three-dimensional space *J. Neurosci.* **8** 2913–27

Simeral J D, Kim S P, Black M J, Donoghue J P and Hochberg L R 2011 Neural control of cursor trajectory and click by a human with tetraplegia 1000 days after implant of an intracortical microelectrode array *J. Neural. Eng.* **8** 025027

Stark E and Abeles M 2007 Predicting movement from multiunit activity *J. Neurosci.* **27** 8387–94

Taylor D M, Tillery S I and Schwartz A B 2002 Direct cortical control of 3D neuroprosthetic devices *Science* **296** 1829–32

Todorova S, Sadtler P, Batista A, Chase S and Ventura V 2014 To sort or not to sort: the impact of spike-sorting on neural decoding performance *J. Neural. Eng.* **11** 056005

Velliste M, Perel S, Spalding M C, Whitford A S and Schwartz A B 2008 Cortical control of a prosthetic arm for self-feeding *Nature* **453** 1098–101

Ventura V 2008 Spike train decoding without spike sorting *Neural. Comput.* **20** 923–63

Wessberg J, Stambaugh C R, Kralik J D, Beck P D, Laubach M, Chapin J K, Kim J and Biggs S J 2000 Real-time prediction of hand trajectory by ensembles of cortical neurons in primates *Nature* **408** 361–5